Scour at a side-weir intersection located on an alluvial river

Fevzi Önen and Hayrullah Agaççioglu*

Yildiz Technical University, Civil Engineering Faculty, Yildiz 34349, Istanbul, Turkey.

*Corresponding author. E-mail: *agacci@yildiz.edu.tr*

Received 1 March 2005; accepted in revised form 27 November 2006

Abstract An experimental investigation of the equilibrium depth of local scour around side-weirs located on an alluvial river is presented in this paper. A sand bar in the middle of the channel and a scour hole close to the weir side is formed because of changes in shear stress field and velocity at the downstream end of the side weir. The depth of clear-water scour increases by time and approaches the equilibrium state asymptotically depending on approach flow velocity. The equilibrium depth of scour increases by the increase of the dimensionless parameters of approach flow velocity, water head ratio, side-weir length and sediment size. Although there is no scour for the dimensionless approach flow velocity less than 0.45, it increases almost linearly with the dimensionless approach flow velocity and the maximum value of scour depth occurs when it is equal to 1.0.

Keywords Alluvial bed; clear-water scour; secondary flow; shear velocity; side-weir

Nordic Hydrology **Vol 38 No 2 pp 165–176** © IWA Publishing 2007

Notations

The following symbols are used in this paper:

b = Width of the channel;
d_{50} = Sediment size at which 50% of material is finer;
g = Acceleration due to gravity;
H = Local scour depth at the side-weir intersection at time t;
H_d = Equilibrium depth of scour at the side-weir intersection;
h = Flow depth at any point in the main channel;
h_1 = Flow depth at the upstream end of the side weir at the centreline of the main channel;
h_2 = Flow depth at the downstream end of the side weir;
J_o = Slope of the channel bottom;
L = Length of the rectangular side weir;
p = Height of weir crest;
Q' = Discharge in the main channel at the downstream end of side weir;
Q_1 = Total discharge in the main channel at the upstream end of side weir;
Q_w = Total flow over side weir;
R = Regression coefficient;
t = Temporal time;
s = Distance along side weir measured from upstream end of side weir;
u_* = Shear velocity;
u_{*c} = Critical shear velocity based on the d_{50} size;
V_1 = Approach mean velocity at the upstream of the side weir in the main channel;
V' = Mean velocity at the downstream of the side weir in the main channel;
V_c = Critical velocity at initiation of motion.

doi: 10.2166/nh.2007.005

Introduction

Side-weirs are widely used in irrigation, land drainage and urban sewerage systems. Many researchers, such as Yu-Tech (1972), Ranga Raju *et al.* (1979), Cheong (1991), Sing *et al.* (1994) and Muslu (2002), are interested in the side-weir flow under the fixed bed conditions. However, there is not enough investigation on side-weir flows on an alluvial bed. The purpose of this study is to determine equilibrium depth of scour around side-weirs for different flow conditions and side-weir dimensions.

As indicated in Figure 1, at sub-critical flow conditions the water surface profile along the weir plane increases from the upstream end towards the downstream end of the side-weir.

El-Khashab (1975) investigated experimentally the secondary flow created by lateral flow and concluded the following:

(1) Starting approximately 0.3 m upstream of the side weir, the velocity on the weir side increases rapidly and it decreases also rapidly on the other side. The peak of this acceleration occurs at half of the weir length from the weir beginning. This acceleration or deceleration causes a rapid increase in super-elevation.

(2) The path of streamlines deviates from its normal course. The volume of water in zone A over the weir crest moves directly towards the side weir and spills over it. In zone B, the volume of water nearly one-third of the weir crest height ($p/3$) tries to join the water in zone A and goes towards the side weir due to the effect of the vertical component of the velocity. The volume of water below $p/3$ in zone B goes onto the main channel (Figure 2).

(3) The low velocity layer occurs dynamically because of diverging flow along the side weir (Region II). The existence of low velocity region pushes the high velocity streamlines towards the side-weir crest and, as a result of this action, a new region is formed (Region I). The volume of water in Region I goes over the side-weir (Figure 3).

(4) The contours of maximum velocities gradually move towards the weir side, causing deceleration in Region III. As can be seen from Figure 3, Region III is formed between Regions I and II. Region III occupies nearly in the middle one-third of the weir height.

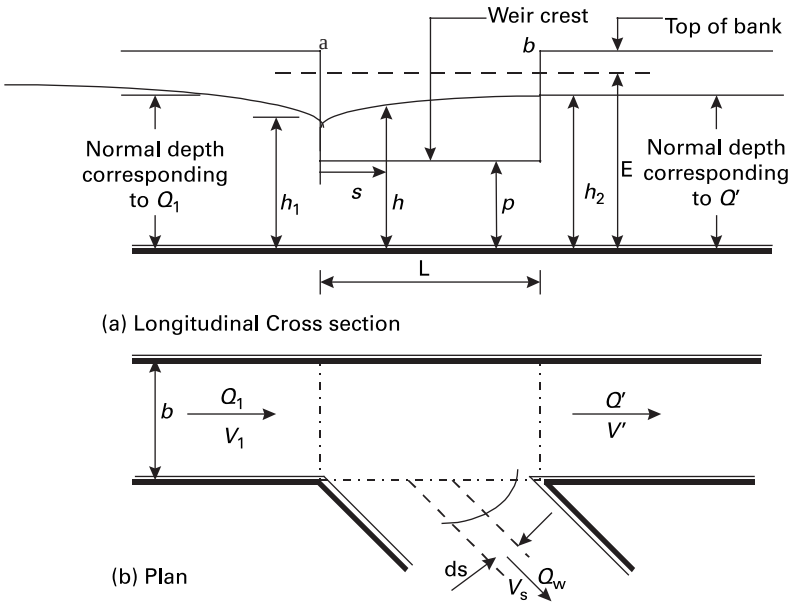

Figure 1 Definition sketch of sub-critical flow over a rectangular side-weir

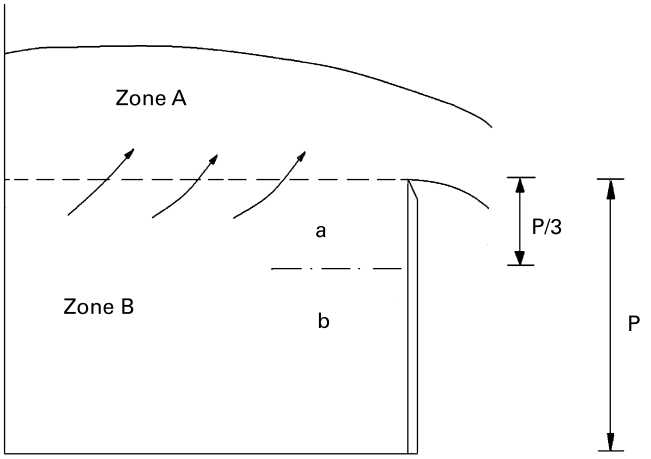

Figure 2 The movement of water along the side weir (El-Khashab 1975)

It is observed that there is a strong secondary flow next to the boundary. This secondary flow next to the boundary causes a contracting of the velocity profiles, forcing the high velocity flow away from the weir wall to crest over the side weir. El-Khashab (1975) defined the intensity of secondary flow created by lateral flow as the percentage ratio of the mean kinetic energy of the lateral motion to the total kinetic energy of the main flow at a given cross section. That means that the intensity of secondary flow depends on the kinetic energy remaining in the main channel.

Fares and Herbertson (1995) investigated the effects of a side overflow channel which is controlled by a broad crested side weir located on the outer side of a 60° channel bend. Their analysis of results showed that continual reductions in shear stresses and velocities occurred at the side overflow region. These reductions were attributed to the development of a separation zone at the upstream corner of the side overflow and a stagnation zone along the inner bank together with strong lateral outward current. The stagnation zone (i.e. low velocity layer) acts to divert and concentrate the longitudinal flow towards the weir side of the main channel. This sets up the conditions in the sections of the main channel downstream of the overflow. The separation zone is responsible for the occurrence of the bed scour along the outer bank at the downstream of the overflow.

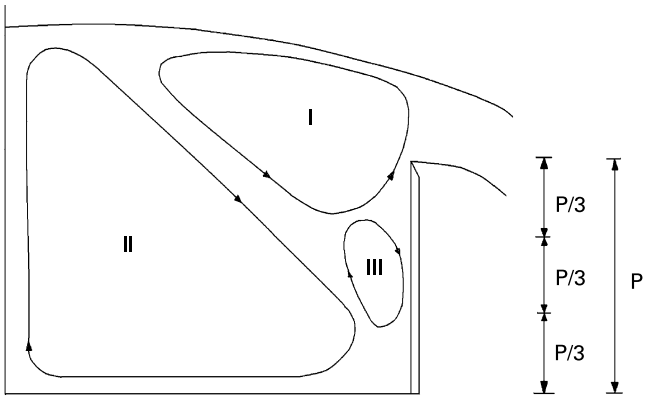

Figure 3 The form of the secondary flow distortions (El-Khashab 1975)

According to Subramanya and Awasthy (1972), El-Khashab (1975), Agaçcioglu and Yüksel (1998) and Agaçcioglu and Cosar (2000), the location and size of the separation zone and reverse flow area depend on the intensity of secondary flow (Figure 4). When the flow velocity or remaining momentum towards the downstream direction in the main channel increases then the reverse flow area and the location of the separation zone move toward the downstream end of the side weir.

Fares (2000) also investigated the characteristic changes in the mechanism of flows in curved channels due to lateral overflows at the cut-off section of a meandering river, Allan Water, by a field study. His results about the main changes in the curved flow behaviour at lateral overflow intersection can be summarized as follows:

(1) The changes in velocity and shear stress distributions depend exactly on the water head ratio, $h_r = (h_1 - p)/h_1$ and the ratio of overflow discharge to main channel discharge, Q_w/Q_1.
(2) These changes are found to be responsible for the initiation of a longitudinal sand bar in the middle of the channel and a deep scour hole close to the outer bank at the downstream of the side overflow section, as can be seen in Figure 5. The characteristics of both longitudinal sand bar and scour hole depend on the overflow rates, Q_w/Q_1, and water head ratio, $(h_1 - p)/h_1$.

Experimental set-up

Experimental studies for determining of the depth of clear-water scour at a side-weir intersection located on an alluvial channel were performed on a rectangular plexiglass flume at the Hydraulic Laboratory of Yildiz Technical University, Istanbul, Turkey. The main flume was 40 cm wide with a 55 cm depth and a well-finished aluminium bottom. The discharge collection flume has 55 cm depth, 50 cm width and is situated parallel to the main flume. Details of the flume are shown in Figure 6. Uniform bed materials were placed as a 20 cm thick layer in the flume with a bed slope of 0.001. The bed of the flume was firstly mixed to prevent sediment grading and layering, and then flattened before each run. During the experiments, the upstream valve was adjusted slowly without causing any disturbance to the bed material until the desired flow condition is obtained in the flume. No sediment inflow was allowed from the upstream due to clear-water conditions.

Side weirs were located at the middle of the the straight part of the main channel. Three different lengths (25, 40 and 50 cm) and three different weir crest height (7, 12 and 17 cm) of the side weir were placed on the side-weir station. The dimensions of side weirs and the ranges of parameters tested were given in Table 1. Side weirs were sharp edged and fully aerated on the overflow side. The water depth was controlled by a sluice gate located at the end of the main flume to produce the uniform flow. Water was supplied from an overhead tank with a constant head and measured by a calibrated 90° V-notched weir (Q_1) at the beginning of the main channel. Another calibrated 90° V-notched weir measured the

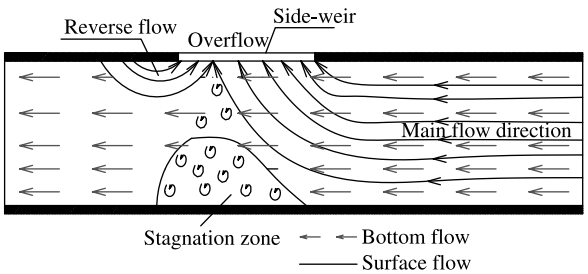

Figure 4 The position of the stagnation zone and reverse flow (Agaçcioglu and Cosar, 2000)

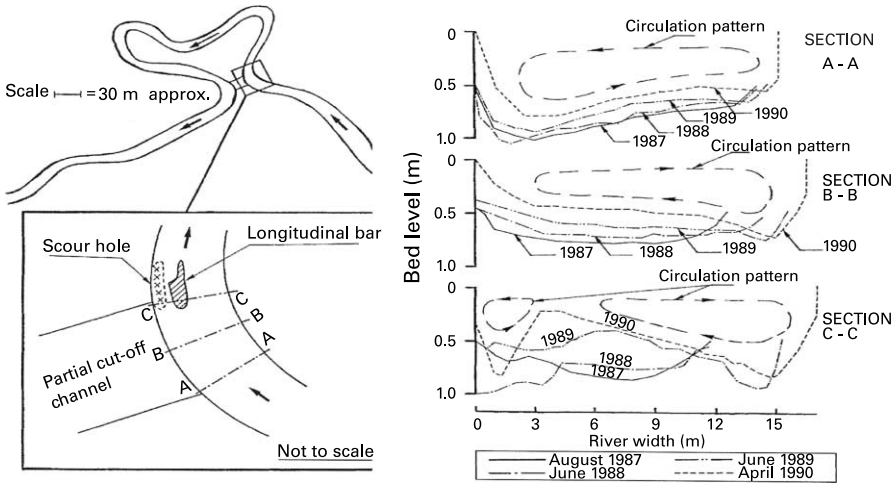

Figure 5 Bed topography profiles in Allan Water at cutoff section (Fares and Herbertson 2000)

side-weir's flow rate (Q_w), which was located at the downstream end of the collection channel. Then, the downstream discharge (Q') in the main channel according to the side-weir location was determined as follows:

$$Q' = Q_1 - Q_w \tag{1}$$

The measurements of water surfaces and bed levels were determined using point gauges capable of reading to the nearest 0.1 mm. The depth of the scour hole was measured at the downstream of side weirs in the main channel (nearly at the centre of the reverse flow area). The mean particle size of bed material (d_{50}) is 1.15 mm. The critical shear velocity, u_{*c}, was determined using the Shields diagram. Melville and Sutherland (1988) give the velocity distribution as follows:

$$\frac{V_c}{u_{*c}} = 5.75 \log\left(5.53 \frac{h_1}{d_{50}}\right). \tag{2}$$

Substituting the value of d_{50} and computed value of u_{*c} for this sediment size, the following equation is obtained:

$$V_c = 0.1556 \log(4809 h_1) \tag{3}$$

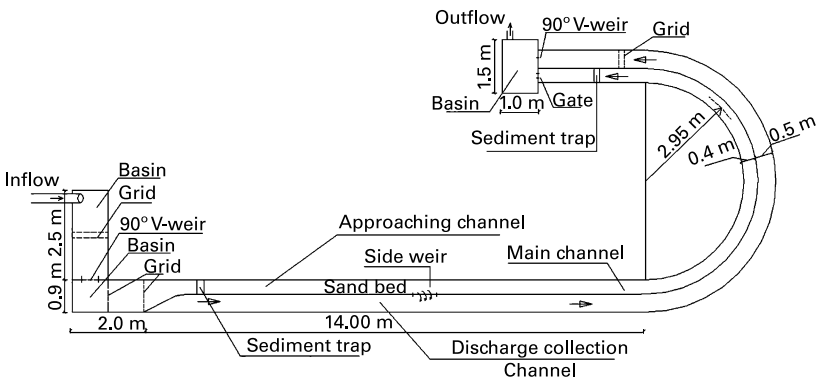

Figure 6 Plan of test flume

Table 1 The dimensions of side-weirs and the ranges of parameters tested

p (cm) (1)	L (cm) (2)	h_1 (cm) (3)	$(h_1 - p)/h_1$ (4)	d_{50}/p (6)	L/b (7)	V_1 (m/s) (8)	V_c (m/s) (9)	V_1/V_c (10)
7	25	12–20	0.45–0.66	0.016	0.625	0.2–0.46	0.43–0.47	0.46–1.0
12	25	19–27	0.37–0.55	0.0096	0.625	0.22–0.49	0.46–0.49	0.47–1.0
17	25	27–33	0.38–0.49	0.0068	0.625	0.3–0.48	0.49–0.5	0.6–1.0
7	40	14–20	0.5–0.63	0.016	1.0	0.22–0.47	0.44–0.47	0.5–1.0
12	40	19–27	0.38–0.56	0.0096	1.0	0.23–0.48	0.46–0.49	0.5–1.0
17	40	24–29	0.30–0.40	0.0068	1.0	0.26–0.48	0.48–0.50	0.55–1.0
7	50	12–18	0.44–0.60	0.016	1.25	0.21–0.46	0.43–0.46	0.49–1.0
12	50	17–24	0.30–0.50	0.0096	1.25	0.21–0.48	0.46–0.48	0.5–1.0
17	50	24–28	0.30–0.40	0.0068	1.25	0.27–0.47	0.48–0.49	0.58–1.0

where V_c is the critical velocity at initiation of sediment motion in m/s and h_1 is the flow depth at the upstream end of the side weir at the flume centre as in m. Equation (3) was used in the computation and it fits well with the experimental observation.

Results and discussion

The bottom topography and location of scour hole

The changes in the main channel bottom topography around side weirs are briefly mentioned according to flow visualization and the obtained bottom topography as given in Figure 7 and Figure 8 when the side weir has $L = 40$ cm and $p = 7$ cm. Flow conditions are summarized in Table 2 for the mentioned figures. Contours in Figures 7 and 8 are illustrated as the thickness of the layer of sand. The reduction in velocities and shear stresses causes the development of stagnation along the inner bank and separation at the upstream corner of the side overflow at the downstream end of the side weir in the main channel. They cause scour at the centre of the reverse flow area. The accumulation in front of the upstream of the side weir and the sand bar behind the scour hole is also observed. As seen from Figure 8, Test run (2) has a higher value of approach flow velocity in the main flow (V_1/V_c) than Test run (1). Therefore the scour depth is deeper. According to observations during experiments, the location of the maximum scour hole moves toward the downstream with an increasing of the dimensionless parameters of approach flow velocity V_1/V_c, water head ratio $(h_1 - p)/h_1$ and the ratio of overflow discharge, Q_w/Q_1. As mentioned above, when the approach flow velocity or remaining momentum towards the downstream direction in the main channel increases then the reverse flow area and the location of scour move toward the downstream end of the side weir.

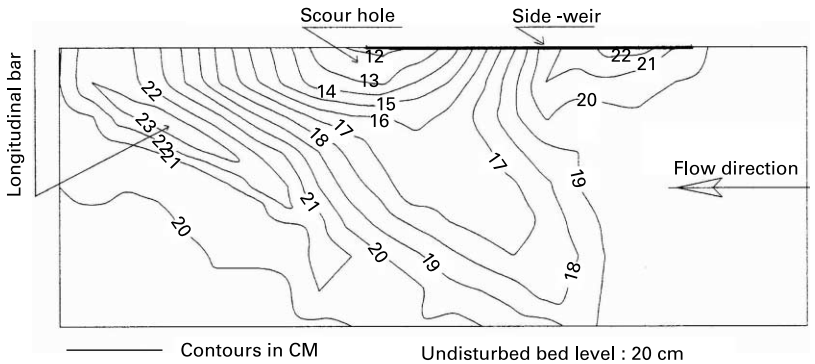

Figure 7 Bed topography at a side-weir intersection when $V_1/V_c = 0.84$, $L = 40$ cm and $p = 7$ cm

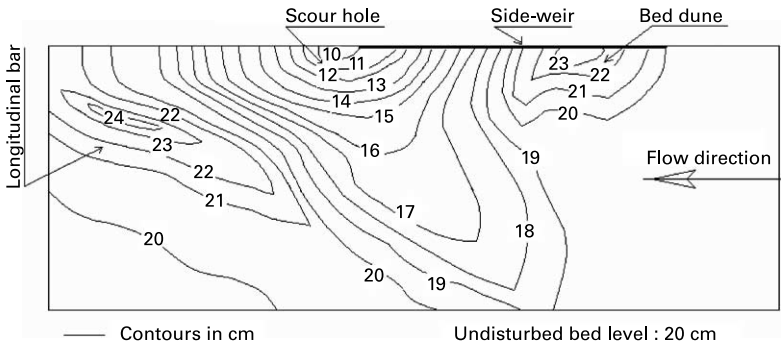

Figure 8 Bed topography at a side-weir intersection when $V_1/V_c = 0.94$, $L = 40$ cm and $p = 7$ cm

Table 2 The flow conditions for Figures 7 and 8

Test run	Q_1 (l/s)	Q_w (l/s)	$Q_r = Q_w/Q_1$ (%)	V_1 (m/s)	V_c (m/s)	V_1/V_c	h_1 m	P m	$(h_1 - p)^*/h_1$
1	25.9	23.2	89	0.38	0.45	0.84	0.170	0.07	0.588
2	31.8	28.5	90	0.43	0.46	0.94	0.185	0.07	0.621

*$h_1 - p$: water head over the weir

Development of scour depth versus time with approach flow velocity

Experiments were carried out to determine the developing of scour depth with time and as a function of approach flow velocity. Each experiment runs for a 12 h period until the rate of development of the scour hole is effectively zero. Figure 9 shows the development of clear-water scour versus time with approach flow velocity as a third parameter for the dimensionless parameters of side-weir length, $L/b = 1.0$ and sediment size, $d_{50}/p = 0.0096$. Figure 9 indicates that the depth of clear-water scour increases by time and approaches the equilibrium state asymptotically depending on approach flow velocity. Time to equilibrium depends on approach flow velocity. When the flow velocity increases, time to the equilibrium depth of scour increases.

Dimensionless parameters

Dimensionless analysis defines the equilibrium depth of scour at the side-weir intersection on an alluvial channel through the following implicit function:

$$\frac{H_d}{p} = f\left(V_1/V_c, L/b, \frac{h_1 - p}{h_1}, d_{50}/p\right) \tag{4}$$

where dimensionless parameters on the right-hand side V_1/V_c, $(h_1 - p)/h_1$, L/b and d_{50}/p represent, respectively, approach flow velocity, water head ratio, side-weir length and sediment size.

Development of equilibrium scour depth with water head ratio

Experiments were carried out to achieve the variations of equilibrium depth of scour, H_d/p, versus the dimensionless water head ratio, $(h_1 - p)/h_1$, with the dimensionless side-weir length, L/b, as a third parameter for all different flow conditions and side-weir dimensions. As can be clearly seen from Figure 10, the equilibrium depth of scour, H_d/p, increases with increasing the water head ratio, $(h_1 - p)/h_1$. The secondary flow next to the weir boundary at the downstream of the weir side causes the scour in front of the side weir. The intensity of

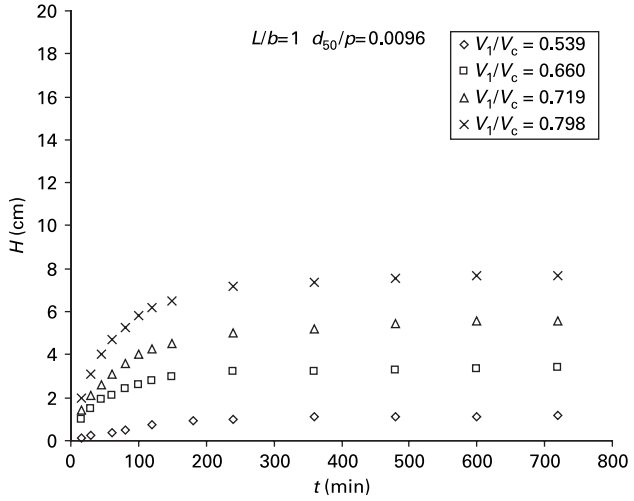

Figure 9 The development of clear-water scour with time when $d_{50}/p = 0.0096$ and $L/b = 1.0$

secondary flow next to the boundary depends on the crest height of the side weir and therefore increases with the dimensionless water head ratio due to the friction of the weir surface (Önen 2005). The intensity of the secondary flow due to decreasing momentum remaining in the main channel is more effective when a side weir is relatively long length. That means that momentum caused by secondary flow towards the direction of the side weir increases when the dimensionless side-weir length (or the overflow length) increases. Scattering of curves for each L/b ratio is attributed to the effect of the dimensionless parameters of sediment size and approach flow velocity.

Development of equilibrium scour depth with approach flow velocity and sediment size

According to our observations, the most expressive parameter about the equilibrium depth of local scour is flow velocity or approach flow velocity. Therefore, experiments are carried out to achieve the equilibrium depth of scour, H_d/p, versus the approach flow velocity, V_1/V_c, with the sediment size, d_{50}/p, as a third parameter including all the different water head

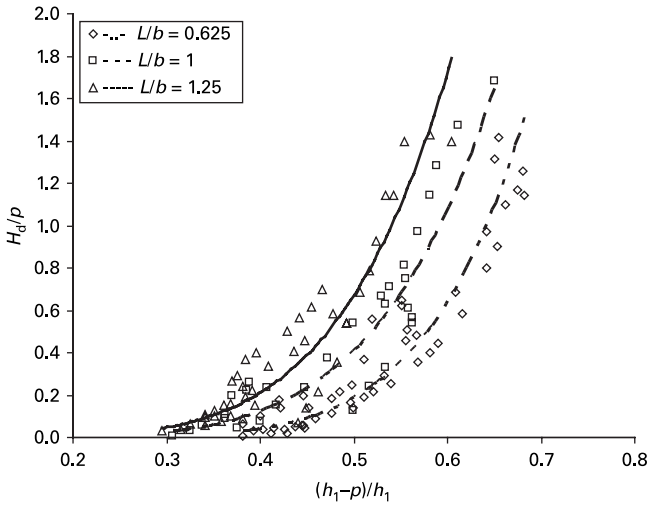

Figure 10 H_d/p versus $(h_1 - p)/h_1$ with L/b

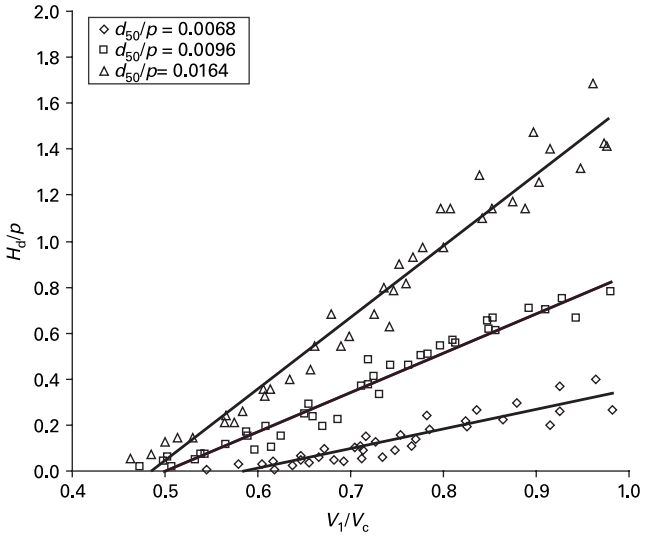

Figure 11 H_d/p versus V_1/V_c with d_{50}/p

ratios, $(h_1 - p)/h_1$, and weir length, L/b, parameters. It is shown in Figure 11 that the equilibrium depth of scour, H_d/p, for all values of sediment sizes d_{50}/p increases almost linearly with an increase in the approach flow velocity. For all the parameter of sediment size d_{50}/p, there is no scour when approach flow velocity is less than 0.45. Thereafter, the equilibrium depth of scour H_d/p increases almost linearly due to an increase in approach flow velocity, V_1/V_c, and the maximum value of scour depth occurs when $V_1/V_c = 1.0$. On the other hand, Figure 11 indicates that the equilibrium depths of scour are close to each other when the approach flow velocity has a small value. However, the divergence of these curves for higher value of approach flow velocity becomes very significant due to the increasing intensity of the secondary flow when the dimensionless side-weir length is relatively high.

The cause of scattering of data points for each ratio of d_{50}/p is the dimensionless parameters of weir length and water head ratio. On the other hand, the equilibrium scour depth H_d/p for the dimensionless sediment sizes, $d_{50}/p = 0.0068$, is smaller than the other

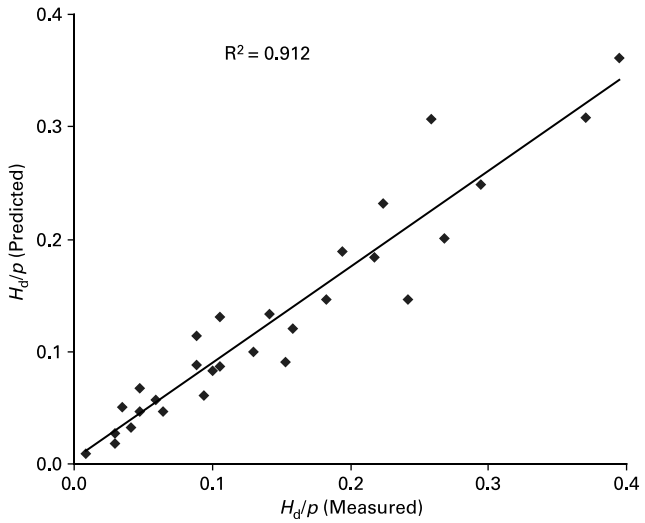

Figure 12 Comparison of actual and predicted values of H_d/p when $d_{50}/p = 0.0068$

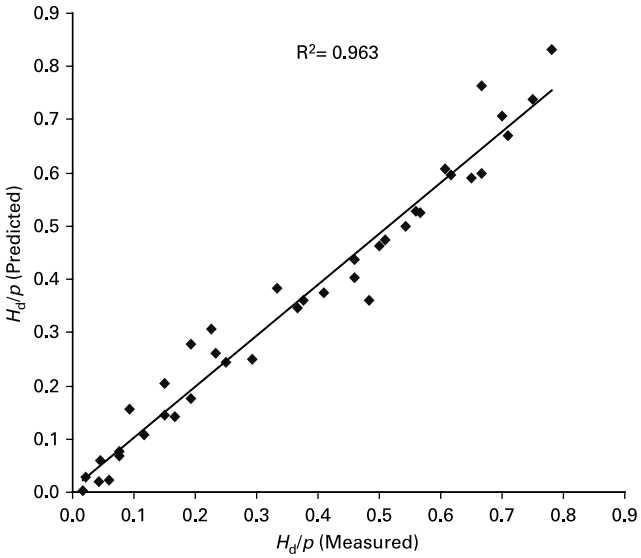

Figure 13 Comparison of actual and predicted values of H_d/p when $d_{50}/p = 0.0096$

values of d_{50}/p due to decrease in the intensity of secondary flow next to the boundary with friction on the weir surface.

As mentioned above, the most important parameters for the equilibrium depth of scour are the dimensionless parameters of approach flow velocity and water head ratio. When regression analysis is applied between H_d/p with V_1/V_c and $(h_1 - p)/h_1$ for different values of d_{50}/p, then the following equations are achieved for the equilibrium depth of scour as follows:

$$\frac{H_d}{p} = \left|9.14\left(\frac{V_1}{V_c}\right)^{0.1} - 8.4\right|^{2.86}\left|\frac{h_1 - p}{h_1} - \frac{V_1}{V_c}\right|^{0.05} \quad d_{50}/p = 0.0068 \;\; R^2 = 0.912 \tag{5}$$

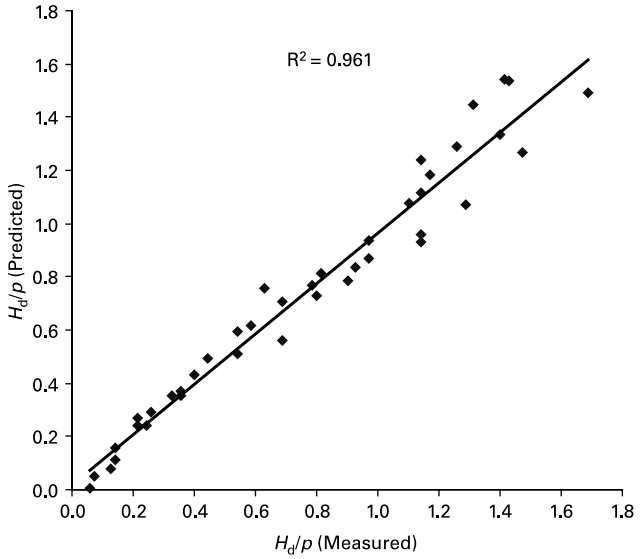

Figure 14 Comparison of actual and predicted values of H_d/p when $d_{50}/p = 0.016$

$$\frac{H_d}{p} = \left|2.69\left(\frac{V_1}{V_c}\right)^{0.55} - 1.79\right|^{1.27} \left|\frac{h_1 - p}{h_1} - \frac{V_1}{V_c}\right|^{0.01} \quad d_{50}/p = 0.0096 \;\; R^2 = 0.963 \tag{6}$$

$$\frac{H_d}{p} = \left|2.64\left(\frac{V_1}{V_c}\right)^{1.13} - 1.09\right|^{1.14} \left|\frac{h_1 - p}{h_1} - \frac{V_1}{V_c}\right|^{0.01} \quad d_{50}/p = 0.0164 \;\; R^2 = 0.961. \tag{7}$$

The performances of Equations (5)–(7) with d_{50}/p ratio are shown in Figures 12–14. The solid lines represent perfect agreement between the predicted and measured values of the equilibrium depth of scour.

Conclusions

The experimental investigations presented herein estimate the equilibrium depth of scour at the side-weir intersection on an alluvial channel bend with different side-weir dimensions in sub-critical flow conditions. The following results can be reached from this study:

(1) The stagnation and separation zones are formed at the side-weir intersection. The separation zone is responsible for the occurrence of the bed scour along the weir side at the downstream of the overflow region.
(2) A longitudinal sand bar in the middle of the channel and a scour hole close to the weir side are formed depending on approach flow velocity, water head ratio, weir length and sediment size.
(3) The depth of clear-water scour increases in time and approaches the equilibrium state asymptotically depending on approach flow velocity.
(4) The equilibrium depth of scour also increases with the increase of the dimensionless parameters of approach flow velocity, water head ratio, side-weir length and sediment size.
(5) There is no scour when the dimensionless approach flow velocity is less than 0.45. Thereafter, the equilibrium depth of scour increases almost linearly with increasing the dimensionless approach flow velocity and attains maximum value of scour at a depth when the dimensionless approach flow velocity is equal to 1.0.

Acknowledgements

This project was financially supported by the research fund of Yildiz Technical University.

References

Agaçcioglu, H. and Cosar, A. (2000). An experimental investigation of side overflow under live bed conditions. *IRTCES, 8th International Symposium on Stochastic Hydraulics, Beijing*, A. A. Balkema, Rotterdam, The Netherlands, pp. 185–190.

Agaçcioglu, H. and Yüksel, Y. (1998). Side-weir flow in curved channel. *ASCE J. Irrig. Drainage Engng.*, **124**(3), 163–175.

Cheong, H.F. (1991). Discharge coefficient of lateral diversion from trapezoidal channel. *ASCE J. Irrig. Drainage Engng.*, **117**(4), 461–475.

El-Khashab, A.M.M. (1975). *Hydraulics of Flow over Side-Weirs.* PhD dissertation, University of Southampton, UK.

Fares, Y.R. (2000). Changes of bed topography in meandering rivers at a neck cutoff intersection. *J. Environ. Hydrol.*, **8**(13), 1–18.

Fares, Y.R. and Herbertson, J.G. (1995). Boundary shear in curved channel with side overflow. *ASCE J. Hydraul. Engng.*, **121**(1), 2–14.

Melville, B.W. and Sutherland, A.J. (1998). Design method for local scour at bridge pier. *ASCE J. Hydraul. Engng.*, **114**(10), 1210–1226.

Muslu, Y. (2002). Numerical analysis for lateral weir flow. *ASCE J. Irrig. Drainage Engng.*, **127**(4), 246–253.

Önen, F. (2005). *An Investigation of Hydrodynamic of Lateral Flows in Movable Bed Rivers*. PhD dissertation, The Technical University of Yildiz, Istanbul, Turkey (in Turkish).

Ranga Raju, K.G., Prasad, B. and Grupta, S.K. (1979). Side-weir in rectangular channel. *ASCE J. Hydraul. Res.*, **105**(5), 547–554.

Singh, R., Manivannan, D. and ve Satyanarayana, T. (1994). Discharge coefficient of rectangular side-weirs. *ASCE J. Irrig. Drain. Eng.*, **120**(4), 814–819.

Subramanya, K. and Awasthy, S.C. (1972). Spatially varied flow over side-weirs. *ASCE J. Hydraul. Engng.*, **98**(1), 1–10.

Yu-Tech, L. (1972). Discussion of spatially varied flow over side-weirs. *ASCE J. Hydraul. Engng.*, **98**(11), 2046–2048.